The 6th European sCO_2 Conference for Energy Systems
April 9-11, 2025, Delft, Netherlands

2025-sCO2.eu-179

THE DEVELOPMENT OF AN SCO_2 TEST FACILITY FOR PARTICLE-TO-SCO_2 HEAT EXCHANGER PERFORMANCE EVALUATION

Bryan J. Siefering
The Pennsylvania State University
University Park, PA, USA

Muhammad Umer
The Pennsylvania State University
University Park, PA, USA

Ellen B. Stechel
Arizona State University
Tempe, AZ, USA

Brian M. Fronk*
The Pennsylvania State University
University Park, PA, USA
bmf141@psu.edu

ABSTRACT

This paper describes the development of a supercritical carbon dioxide test facility to mimic the primary heat exchanger inlet operation conditions of a recompression sCO_2 Brayton cycle. The experimental facility is used to test and evaluate the heat transfer performance of a particle-to-sCO_2 heat exchanger for concentrated solar power applications. The sCO_2 flow loop is comprised of five main components: a positive displacement gear pump, piston accumulator, sCO_2 preheater, experimental test section, and sCO_2 post cooler. The test facility is instrumented with measurement devices to quantify the heat and mass flows within the system. The loop operates at isobaric conditions up to 20 MPa and is split into a hot and cold side. On the cold side, the sCO_2 is cooled below room temperature by the post cooler, increasing the density of the sCO_2 high enough such that it can be circulated using the gear pump. The 10.8 kW preheater delivers sCO_2 to the test section at temperatures up to 600°C at flow rates up to 0.013 kg s^{-1}. Within the test section the sCO_2 is further heated by inert CARBO HSP 40/70 particles. The development of the novel particle-to-sCO_2 heat exchanger is also reported in this work. The heat exchanger was tested at dilute and dense flow conditions in the particle domain. The heat transfer performance and particle-to-sCO_2 recovery effectiveness are characterized and compared to model predictions. By validating the model with the collected experimental data, it can be used to guide the design of future larger scale particle-to-sCO_2 heat exchangers.

INTRODUCTION AND PRIOR WORK

Supercritical carbon dioxide Brayton cycles have received significant attention for use in concentrated solar thermal power plants [1]. In these and other applications, the sCO_2 Brayton cycle will need to be integrated with thermal storage. Inert or reactive particle-based storage has many advantages such as high energy density, stability at high temperatures, and low material cost. However, there is a thermal bottleneck in transferring sensible and chemical energy stored in particles into high pressure, high temperature sCO_2. There has been significant work on particle-to-SCO_2 heat exchanger using moving packed bed [2], [3], [4], [5] or fluidized bed heat exchangers [6], [7], [8], [9], [10], [11], [12], [13].

Our research group has considered an alternative approach where gravity driven, reacting particles with solid volume fraction of less than 1% fall through a finned tube heat exchanger. Oxidizing air flows in counterflow in direct contact with the particles. Energy is transferred from the particle/air mixture to the sCO_2 flowing in tubes via conduction, radiation and convection. Initial thermodynamic [14] and thermal hydraulic [15] investigations were used to establish the operating conditions and required heat transfer area to achieve effective heat transfer from redox-active particles to sCO_2 at conditions relevant concentrated solar power plants. These studies guided the development of an initial prototype device (Figure 1). Experiments at temperatures greater than 400°C were conducted using inert particles and air instead of sCO_2 as the heat transfer fluid to validate the thermal and hydraulic models [16]. The next steps in this research are to use sCO_2 as the heat transfer fluid with inert and then reacting particles.

Thus, the objective of this paper is to develop and demonstrate a supercritical carbon dioxide test facility that can be used to simulate the inlet conditions of a primary heat exchanger in a recompression Brayton cycle. The facility is designed to provide sCO_2 at temperatures up to 600°C for a prototype heat exchanger with capacity up to 10 kW. The operational limits of the facility are confirmed and then

* corresponding author(s)

DOI: 10.17185/duepublico/83285

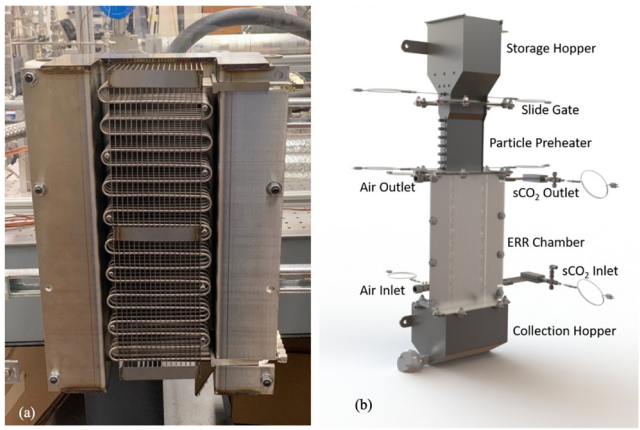

Figure 1: (a) Photograph and (b) rendering of particle-to-air heat exchanger from Siefering [16].

experiments conducted using a scaled down version of the particle-to-sCO_2 heat exchanger shown in Figure 1.

SUPERCRITICAL FLOW LOOP

The purpose of this test facility is to simulate the high inlet temperature and pressure conditions of a primary heat exchanger in a sCO_2 recompression Brayton cycle. The test loop is divided into a hot and a cold side and operates at a constant pressure above the critical point. Carbon dioxide is circulated using a positive displacement pump rather than a compressor. Figure 2 shows a schematic and photograph of the experimental facility, which consists of main components:

1. A positive displacement gear pump for circulating low temperature, "liquid-like" sCO_2.
2. A piston accumulator coupled to a high-pressure nitrogen gas bottle for maintaining the working pressure of the experimental facility.
3. A preheater for increasing the sCO_2 temperature to the required inlet conditions for the test section.
4. The test section (described in the following section)
5. A post cooler for reducing the fluid temperature to the cold-side temperature.

The fluid circulates through the facility using a variable speed Micropump GC-M35 positive displacement gear pump (PN: L27276), which displaces 3.48 mL per revolution. The pump operates at a maximum speed of 4000 RPM, providing a maximum differential pressure of 0.51 MPa and maximum working pressure of 20.7 MPa. It is driven by a 0.5 horsepower variable speed AC motor from Baldor (PN: CM3537) via a magnetic coupling, which eliminates the need for seals and lubricants in the pump head. The pump motor speed is controlled by an Eaton variable frequency drive (PN: DC1-1D2D3NN-AS6CE1). To adjust the system pressure, an Accumulators Inc. piston accumulator (PN: PA1QT31004B10G3FK) with a maximum allowable working pressure (MAWP) of 20.7 MPa is coupled to a high-pressure nitrogen gas bottle. Pressurizing the piston with N_2 changes the system volume and pressure.

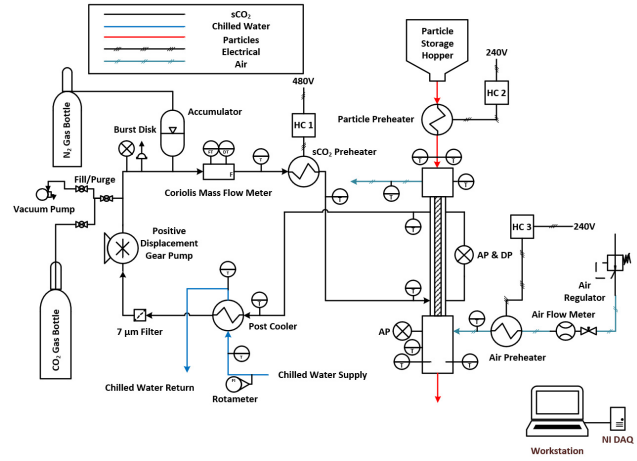

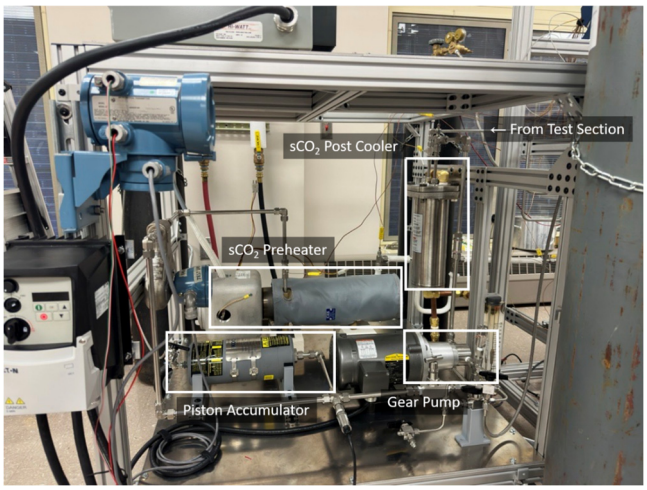

Figure 2: (top) Schematic and (bottom) photograph of the sCO_2 experimental facility.

After leaving the pump, the sCO_2 is heated in an adjustable power 10.8 kW Cast Aluminum Solutions CAST-X HT 2500 circulation heater (PN: BX17A5N-107A) up to the desired test section inlet temperature. This heater operates on 3-phase 480V and is controlled using a custom Hi-Watt inc. heater control console with a Watlow DIN-A-MITE solid state power controller and a Watlow F4T PID controller. The sCO_2 preheater has 3 cartridge heaters wired in a 3-phase delta configuration. Within the heater, fluid flows through a coiled 12.7 mm (0.5 in) OD Inconel 600 tube with wall thickness of 1.65 mm (0.065 in). Both the coiled tube and cartridge heaters are cast into a bronze enclosure to apply uniform heat flux to the tube. The preheater is insulated with an insulating jacket provided by the manufacturer, and the tubing from the preheater to the test section is insulated with > 50 mm of high temperature ceramic fiber insulation. The maximum continuous operational temperature of the heater is 600°C, and the tube rated pressure is based on the ASME B31.3 guidelines (ASME, 2022). At 538°C, the manufacturer rated maximum pressure is 18.7 MPa, but the pressure can exceed 20 MPa at temperature less than 500°C.

DOI: 10.17185/duepublico/83285

Table 1: Summary of sCO_2 experimental facility instrumentation.

Variable	Manufacturer/Model Number	Range	Uncertainty
sCO_2 Mass flow	Micromotion (CMF010M Elite)	-5 to 15 g s^{-1}	±0.2%
Temperature	K type thermocouples (Omega)	-200 to 1260°C	Max of ±2.2°C or ±0.75%
Absolute pressure	Rosemount 3051SMV	0.03 to 15 MPa	±0.035% of span
Gauge pressure	Omega (PX309-3KGI)	0 to 20.7 MPa	±0.08% of range
Differential pressure	Rosemount 3051SMV	-5 to 5 kPa	±0.035% of span
Counterflow air flow rate	King Instrument Company Rotameter	2 to 20 SCFM	±2% of full-scale

The tubing from the preheater to the test section used 12.7 mm (0.5 in) 316 stainless steel tubing with a wall thickness of 1.65 mm (0.065 in). This tubing is rated for pressure up to 15 MPa at 600°C, exceeding the maximum operational limit of the facility. Thermal expansion within the sCO_2 facility was accommodated with expansion loops in the straight runs of tubing to allow for tube deflection without significant buildup of stress. The test section used in the initial experiments is described in the next section.

The outlet of the test section is the highest temperature in the test facility. To handle this high-temperature zone, 9.52 mm (0.375 in) diameter Inconel 625 tubing with a 1.65 mm (0.065 in) wall thickness is used between the test section outlet and the post cooler inlet. Stainless steel Swagelok fittings connect the tubing from the test section to the post cooler tubing. This section is un-insulated to allow some heat rejection before the fluid enters the post cooler.

The post cooler is a Sentry Equipment double helical sample cooler (Model: FLR-62B3). This shell and tube heat exchanger has a heat transfer area of 0.33 m². The fluid flows through a 9.52 mm (0.375 in) outer diameter Inconel 625 tube with a 0.90 mm (0.035 in) wall thickness. The manufacturer's pressure rating for this cooler is 23.4 MPa at 593°C. The shell side, made of 304 stainless steel, is coupled with building chilled water supply for heat rejection. The chilled water line operates at a maximum flow rate of 45 L min^{-1} GPM with an inlet temperature between 9-12°C. A temperature increase of 5°C in the water line is acceptable, giving the heat exchanger a heat rejection capability of nearly 20 kW. After the post cooler, the fluid passes through a 7 µm mesh before re-entering the pump.

All fittings on the facility are stainless steel Swagelok compression tube fittings or NPT-to-Swagelok. Swagelok tube fittings are rated to exceed the pressure of the tubing to which they are connected, therefore following ASME B31.3 guidelines on the tubing also qualifies the fittings. The facility is built on a combination of a rolling aluminum extrusion cart and tower. The entire facility is enclosed in impact resistance 6.35 mm thick polycarbonate sheet for safety.

The facility is instrumented to measure sCO_2 temperatures, absolute and differential pressure, and mass flow rate through the system. A summary of instrumentation is shown in Table 1.

A Micromotion Coriolis flow meter (MN: CMF010M Elite) measures the mass flow rate and density of the sCO_2 on the cold side of the facility. The mass flow meter is configured for a range of -5 to 15 g s^{-1} and a density range of 0 to 1100 kg m^{-3}. A Micromotion 2700 transmitter sends analog 4 to 20 mA signals to a National Instruments data acquisition system. The MAWP of the mass flow meter is 12.7 MPa, making it the limiting pressure component in the facility. To protect this instrument, the operational pressure limit of the facility is set to less than 10 MPa.

SUPERCRITICAL FLOW LOOP OPERATIONAL LIMIT TESTING

A series of experiments were conducted to assess the operational limits of the sCO_2 test facility. The heat exchanger described in the next section was installed, but there was no air or particle flow on the tube-side. The maximum preheater process temperature was set to 550°C. The mass flow rate of sCO2 was set to 13 g s^{-1}, allowing the preheater to operate at the full 10.8 kW capacity when heating the fluid from approximately 12°C to more than 500°C at a pressure of 9.3 MPa. The operating pressure is limited by the 12.3 MPa maximum allowable pressure of the Coriolis mass flow meter. All other components in the loop are rated up to 20 MPa to enable future higher temperature testing with a new mass flow meter. Table 2 shows measured temperatures at each location in the test facility and Table 3 shows measured and calculated heat addition/rejection calculated using the mass flow rate and the inlet and outlet specific enthalpies evaluated from the measured temperature and pressure using the equation of state from Span and Wagner [18].

During the experiment, the preheater was set to 100% power which is 10.8 kW_e per the manufacturer. The calculated heat input to the sCO_2 versus the rated power of the heater is only 4.4% difference. This discrepancy can be attributed to heat loss through the preheater insulation, which reached a surface temperature of 48°C, as well as variations in inlet voltage from the nominal 480V. Approximately 360 W of energy was lost

Table 2: sCO_2 facility operational limit steady state temperatures at mass flow rate of 13 g s^{-1} and pressure of 9.33 MPa

Location	Temperature (°C)
Post Cooler Outlet	10.2
Preheater Inlet	13.1
Preheater Outlet	531.9
Test Section Inlet	509.0
Test Section Outlet	501.5
Post Cooler Inlet	465.8

DOI: 10.17185/duepublico/83285

Table 3: Component/tubing heat addition/loss during operational limit steady state mass flow rate of 13 g s^{-1} and pressure of 9.33 MPa

Component/location	Heat Transfer (kW)
Preheater	10.34
Preheater to test section tubing	-0.358
Test section	-0.117
Test section to post-cooler tubing	-0.553
Post-cooler	-9.41
Post-cooler to preheater tubing	0.092
Net heat transfer	*0.0*

through the tubing from the preheater to the test section, with tube surface temperatures reaching more than 500°C.

Approximately 552 W of energy were rejected from the uninsulated tubing connecting the test section and the post-cooler, reducing the required thermal load of the heat exchanger. The post cooler transferred 9.4 kW of energy to the building chilled water line. Water flows through the shell side of the post cooler at 45 L min^{-1}, with an inlet temperature of 10.0°C and outlet temperature of 13°C.

This test demonstrated the capability of the test loop to safely achieve target test heat exchanger inlet temperatures of more than 500°C at pressures of nearly 10 MPa. The tests also verified the heating capacities of the preheater and water-coupled post cooler, and that the system instrumentation could be used to calculate consistent energy balances of each component to characterize heat loss.

PARTICLE HEAT EXCHANGER PROTOTYPE

The test facility was then used to conduct experiments on a particle-to-sCO_2 prototype heat exchanger was designed to simulate the conditions of an energy recovery reactor for thermochemical energy storage. Here dilute flows of less than 1% volume fraction of hot, redox-active particles are re-oxidized with air and transfer energy via conduction, convection and radiation to high pressure sCO_2 contained in tubes. In this study, experiments are conducted with inert particles to validate thermal hydraulic models of the prototype heat exchanger. A rendering of the tube-in-tube particle heat exchanger prototype is shown in Figure 3.

The prototype is fabricated entirely from 306 and 316 stainless steel components. To impede the path of the particles and increase the residence time while maintaining dilute flow conditions, a 62.9-cm-long tube with a 32-blade static mixing element inside was used as the inner tube. The outer diameter of the static mixing tube is 12.7 mm (0.5 in) with a wall thickness of 0.90 mm (0.035 in).

Bored-through Swagelok compression tube fittings create the pressure boundary between the inner and outer tubes, resulting in an annulus for the counterflow of sCO_2 and gravity-driven particle flow. The outer tube is a 40.6 cm long, 19.05 mm

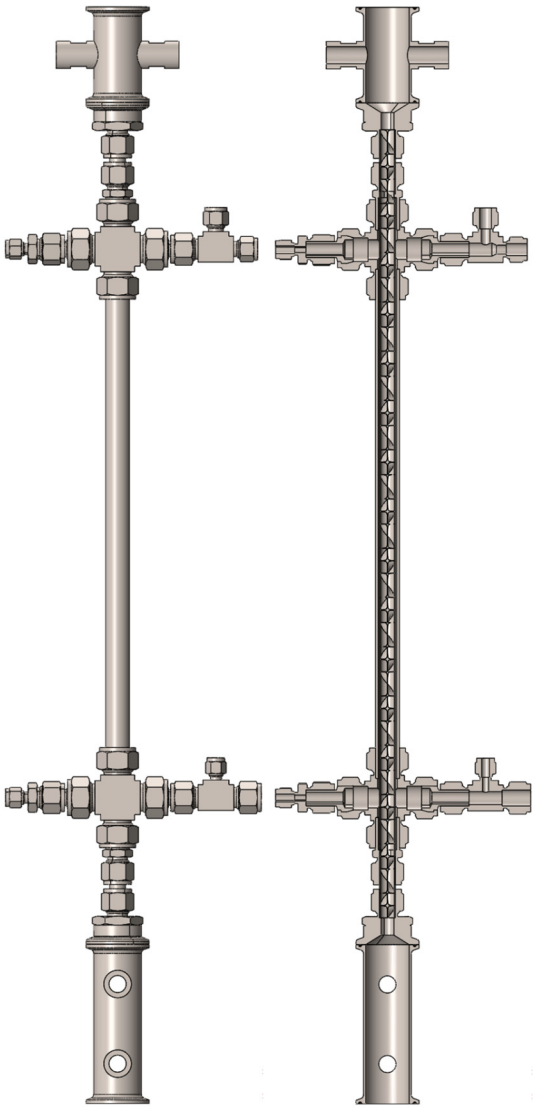

Figure 3: Rendering and cross section of the particle heat exchanger prototype.

(0.75 in) outer diameter 316 stainless steel tube with a wall thickness of 2.1 mm (0.083 inches). When assembled, the hydraulic diameter of the annulus for the sCO_2 annulus is 1.04 mm.

At the top and bottom of the static mixing tube, a Swagelok to 1.5-inch tri-clamp adapter couples the particle/air flow to temperature measurement sections.

PARTICLE HEAT EXCHANGER EXPERIMENTAL APPROACH

The sCO_2 test facility and particle heat exchanger prototype were used to conduct experiments with inert CARBO HSP 40/70 particles with a size range of 212 to 425 µm, median diameter of 332 µm and with a particle density of 3,610 kg m^{-3}. Here, 77.3% of the particles' diameter ranged between 300-350 µm [19].

DOI: 10.17185/duepublico/83285

Experiments were conducted for three different operational modes:

1. **Dilute:** Particles at a solid volume fraction of approximately 1% fell through the heat exchange via gravity with no forced counterflow of air.
2. **Counterflow:** Particles at solid volume fraction of approximately 1% fell through the heat exchanger via gravity with varying flow rates of counterflow air. Velocity is maintained below the entrainment velocity of the particles.
3. **Moving Packed Bed:** Particles at near maximum packing condition with a high solid volume fraction (~43%) and no air counterflow air flowed through the heat exchanger.

For each mode, experiments were conducted at particle inlet temperatures of 350°C and 530°C, and sCO_2 inlet temperatures of 100°C and 200°C. All experiments were conducted at a fixed mass flow rate of particles of 0.89 g s^{-1}, mass flow rate of sCO_2 of 5 g s^{-1} and inlet pressure of sCO_2 between 8.5 and 8.8 MPa.

Before conducting the dilute particle flow experiments, the average velocity of particles flowing through the static mixing tube was measured to be 0.1796 ± 0.01 m s^{-1} by recording the time it took for particles to fall through the tube from inlet to outlet, allowing the residence time to be calculated. The average residence time recorded was 3.5 seconds across 15 trials, with a conservative uncertainty of ±0.2 seconds to account for human bias. These measurements were repeated with counterflow air and found to be equal to the dilute case. The particle solid volume fraction for both cases were calculated from the particle residence time, reactor height, particle density, and the cross-sectional area of the center tube. The calculated particle solid volume fraction was 1.66% ± 0.2%, from Equation 1.

$$\epsilon_{\mathrm{p}} = \frac{\dot{m}_{\mathrm{p}}}{(L/t_{\mathrm{res}})\rho_{\mathrm{p}} A_{\mathrm{flow}}} \tag{1}$$

The counterflow experiments were conducted under the same particle conditions but with counterflow air in the center tube to simulate the reacting flow scenario. The inlet temperature of the counterflow air was set equal to the sCO_2 inlet temperature to prevent parasitic heat transfer from the sCO_2 flow into the air stream. Thus, particles are the only heat source for both sCO_2 and air. For experiments with 100°C sCO2 and air inlet temperatures, the air flow rate was set to 8 slm, while for 200°C inlet temperature experiments, the air flow rate was set to 4 slm to prevent particle entrainment. The measured residence time of particles was the same as in the 'Dilute' case, so the same solid volume fraction was assumed.

For the moving packed bed experiments, the orifice plate in the particle preheater was removed, causing the entire test section to fill with particles. The flow was controlled with a single orifice plate at the bottom of the test section. Multiple experiments at varying particle column height above the orifice plate were conducted to confirm that the mass flow rate was not affected. During operation, there were no signs of ratholes or change in mass flow due to funneling. The absence of funnel flow was verified with a section of sight glass tubing.

Data were collected at steady state for each operational scenario for different particle and sCO_2 inlet temperatures. Steady state was defined as a less than 1°C variation over a 5-minute runtime, the duration of data collection for each experiment. Measurements using the instruments described in Table 1 are used to calculate the energy transferred into/out of the particles, air, and sCO_2, as described in the next section.

DATA ANALYSIS AND RESULTS

Equation (2) is used to determine the heat transfer from the particles.

$$\dot{Q}_{\mathrm{p}} = \dot{m}_{\mathrm{p}}\left(h_{\mathrm{p,in}} - h_{\mathrm{p,out}}\right) \tag{2}$$

The mass flow rate of particles in all cases was constant at 0.89 ± 0.1 g s^{-1}, which was measured using an Ohaus mass scale (MN: Ranger 3000). The flow rate of the CARBO particles through the orifice plate used at the inlet of the test section was measured using automated mass measurements from the scale to a computer at an interval of 5 seconds prior to installation to avoid hot particles on the scale for long durations. During experiments, the mass flow rate was monitored and confirmed by periodic catch and weigh tests using the same scale. The resolution of the scale is 0.1 g, and the linearity is reported at ±0.1 g, therefore an uncertainty of ±0.1 g s^{-1} is applied to the scale.

Calculating the change in specific enthalpy of the particle stream involves measuring the inlet and outlet temperatures of the particles. Since thermodynamic data for CARBO HSP 40/70 are not readily available, the change in specific enthalpy must be calculated rather than referenced. The specific heat of the particles is not constant over the temperature range from inlet to outlet. Therefore, to calculate the change in specific enthalpy, the specific heat must be integrated over the temperature range, as shown in Equation (3).

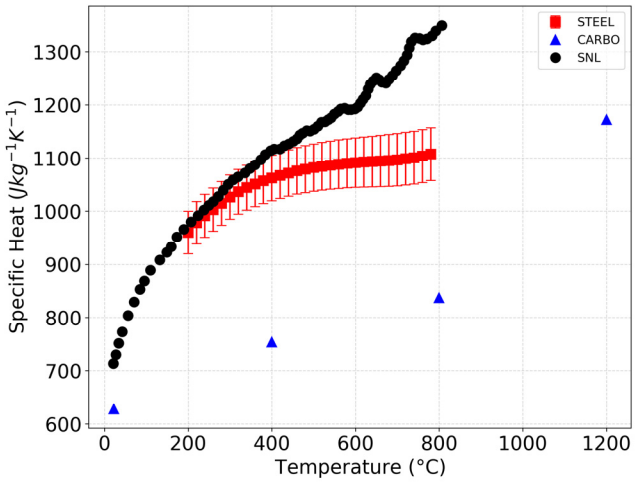

Figure 4: Specific heat data versus temperature data from SNL [20], STEEL Lab [21] and CARBO [22].

DOI: 10.17185/duepublico/83285

$$\left(h_{\mathrm{p,in}} - h_{\mathrm{p,out}}\right) = \int_{\mathrm{T_{p,out}}}^{T_{\mathrm{p,in}}} c_{\mathrm{p}}(T)dT \qquad (3)$$

Specific heat data for CARBO HSP 40/70 reported in Siegel et al. [20] from Sandia National Lab (SNL), STEEL Lab [21] from Georgia Tech, and CARBO [22] the manufacturer of the particles. Figure 4 shows the specific heat data plotted versus temperature for all three datasets.

The data from SNL and STEEL show close agreement at temperatures ranging from 200°C - 420°C. The data from SNL with a ±10% uncertainty is used in this analysis. A 4th degree polynomial fit of the data is evaluated as the integrand in Equation (3) to calculate the change in specific enthalpy of the particle stream.

Figure 5 shows the calculated particle heat transfer rates for the different operational modes and particle and sCO_2 inlet temperatures. The experimental uncertainty calculated using the method described by Kline and McClintock [23] and the manufacturer reported instrument uncertainties with a 95% confidence interval. For the 100°C sCO_2 temperature experiments, raising the particle inlet temperature ~52% from the low value of (350°C to 360°C) to the high particle temperature (530°C to 550°C), resulted in an increase of 167%, 85%, and 90% in the heat transfer rate to the particles in the dilute without counterflow air, dilute flow with counterflow air, and moving packed bed flow, respectively. Similar non-linear increase in heat transfer rate with increasing particle-to- sCO_2 temperature were observed at the 200°C sCO_2 inlet. The non-linear change can be attributed to the increased effectiveness of radiative heat transfer at higher temperatures.

When the particle temperature is maintained and the sCO_2 temperature is increased, the heat transfer rate decreases in all cases due to the lower driving temperature difference between the particles and the wall. The moving packed bed experiments show the highest heat transfer rate from the particle stream while operating at the same particle mass flow rate. This is because the packed particles maximize contact area with the wall and are well mixed within the heat exchanger due to the static mixing tube. Dilute flow with counterflow gas exhibits higher heat transfer rates from the particle stream due to convective heat transfer with the air stream.

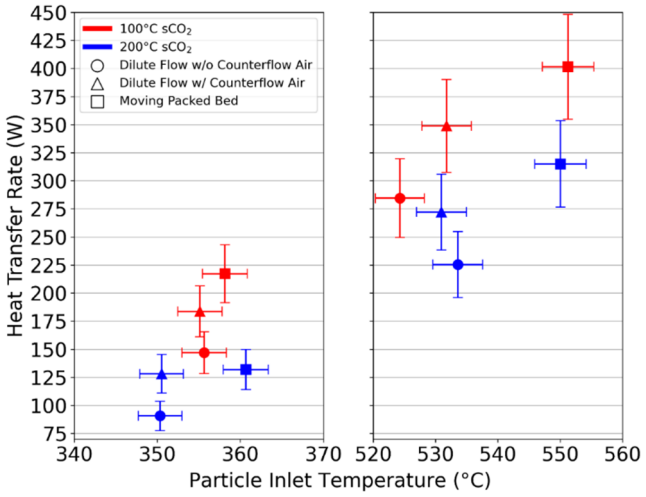

Figure 5: Particle stream heat transfer rates at different operational conditions.

The heat transfer rate to the sCO_2 is calculated using Equation (4). Here, the specific enthalpy values of the sCO_2 stream are calculated from equation of state for carbon dioxide from Span and Wagner [18]. Figure 6 shows the experimental results for the different operational conditions.

$$\dot{Q}_{\mathrm{sCO_2}} = \dot{m}_{\mathrm{sCO_2}}\left(h_{\mathrm{sCO_2,out}} - h_{\mathrm{sCO_2,in}}\right) \qquad (4)$$

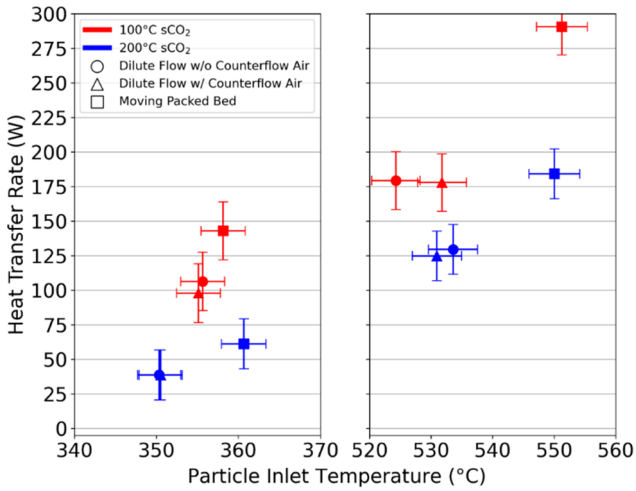

Figure 6: sCO_2 heat transfer rates at different operational conditions.

A notable trend is the effect of counterflow air on heat transfer rates. For the particles, counterflow air significantly increases the heat transfer rate compared to purely dilute flow. In contrast, sCO_2 heat transfer rates show significant overlap between experiments with and without counterflow air, indicating that convection from the air stream does not significantly aid heat transfer to sCO_2 in the annulus.

Moving packed bed experiments consistently show the highest heat transfer rates. Increasing the driving temperature difference leads to increased heat transfer rates in all cases.

Finally, the overall particle-to-sCO_2 heat transfer coefficient can be calculated using Equations (5) and (6) [24]. The hot stream and cold streams in the log mean temperature difference (LMTD) calculation are the particle and sCO_2 temperatures respectively, denoted by h and c in Equation (6).

$$U = \frac{\dot{Q}}{A\ LMTD} \qquad (5)$$

$$\text{Where, } LMTD = \frac{\left(T_{\mathrm{h_{out}}} - T_{\mathrm{c_{in}}}\right) - \left(T_{\mathrm{h_{in}}} - T_{\mathrm{c_{out}}}\right)}{\ln\frac{\left(T_{\mathrm{h_{out}}} - T_{\mathrm{c_{in}}}\right)}{\left(T_{\mathrm{h_{in}}} - T_{\mathrm{c_{out}}}\right)}} \qquad (6)$$

DOI: 10.17185/duepublico/83285

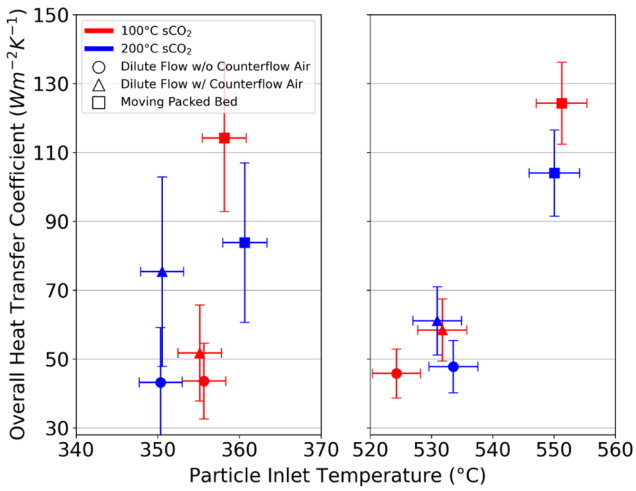

Figure 7: Overall heat transfer coefficients at different operational conditions.

The heat transfer rate of the sCO_2 domain is used as the $\dot{Q}$ in Equation (5) because it is the heat transfer rate of interest in the heat exchanger. The measured steady state heat loss of the sCO_2 flow without particles was added to sCO_2 heat transfer rate, as the particles transferred enough heat to the heat transfer fluid to overcome the heat loss. For 100°C sCO_2 flow at 5 g s^{-1}, the test section lost heat at 13.54 W, while at 200°C the heat loss increased to 30.01 W. The heat transfer area is calculated from the product of the circumference of outside of the center static mixing tube and the length between the inlet and outlet sCO_2 connections. In this analysis, the heat transfer area is 0.01756 m^2. Figure 7 shows the measured heat transfer coefficients.

Heat transfer coefficients of approximately 45 W m^{-2} K^{-1} were measured for all four cases of dilute particle flow without counterflow air. Increasing the particle inlet temperature resulted in a slight increase in the overall heat transfer coefficient: 5% for 100°C sCO_2 cases and 10% for 200°C cases, due to increased radiative heat transfer from the particles [25]. Adding counterflow air further increased the overall heat transfer coefficient, not because of increased heat transfer to the sCO_2, but due to a lower LMTD. The LMTD decreases as the particle outlet temperature drops further from convection heat transfer with the incoming counterflow air. The uncertainty bars in the left plot of Figure 6 are large due to the relatively low temperature differences measured in the heat exchanger during experiments. Despite the increased uncertainty of type K thermocouples at higher temperatures, the higher particle inlet temperature cases show less experimental uncertainty due to larger temperature differences, especially in the sCO_2 inlet and outlet temperatures.

Overall heat transfer coefficients as high as 125 W m^{-2} K^{-1} were measured during the moving packed bed experiments, where the driving temperature difference was the largest, resulting in the highest sCO_2 heat transfer rate. Similar heat transfer coefficients of 50-80 W m^{-2} K^{-1} in moving packed bed heat exchangers were reported by Albrecht et al. [26] before optimizing the heat exchanger with smaller characteristic lengths in the particle flow channels, increased surface area, and micro-pins to enhance sCO_2 heat transfer [27]. The static mixing tube enhances heat transfer by increasing particle and air mixing throughout the heat exchanger. However, the mixing element is only spot welded at the ends and not continuously bonded to the tube wall, so it does not act as a fin or provide additional heat transfer area in the center tube. Heat transfer rates and coefficients could be further increased by incorporating additional heat transfer area in the center tube.

MODEL APPROACH AND RESULTS

Siefering reports the development of a discretized thermal resistance network model, which accounts for particle hydrodynamics, multi-mode heat transfer, and reaction equilibrium [16]. They validated the thermal and hydraulic sub models with experiment using inert particles and air as the heat transfer fluid for the prototype device shown in Figure 1.

This model is updated here to reflect the particle-to-sCO_2 heat exchanger shown in Figure 3. Unlike the prior work, the particle and air domains are assumed to have the same temperature due to the static mixing, based on the work of Frain et al. [28] and Rajan et al. [29]. The simplified energy balances for the particle/air and sCO_2 domain are shown in Equations (7) – (9).

$$\dot{m}_\mathrm{p} c_{\mathrm{p,p}} T_\mathrm{p} + \dot{m}_\mathrm{p} c_{\mathrm{p,p}} dT_\mathrm{p} = \dot{m}_\mathrm{p} c_{\mathrm{p,p}} T_\mathrm{p} + d\dot{q}_\mathrm{rad} + d\dot{q}_\mathrm{a,w} + d\dot{q}_\mathrm{rxn} + d\dot{q}_\mathrm{loss,air} + d\dot{q}_\mathrm{loss} \quad (7)$$

$$d\dot{q}_\mathrm{a,w} + d\dot{q}_\mathrm{rad} = d\dot{q}_\mathrm{w,c} \quad (8)$$

$$\dot{m}_\mathrm{c} c_{\mathrm{p,c}} T_\mathrm{c} + d\dot{q}_\mathrm{w,c} = \dot{m}_\mathrm{c} c_{\mathrm{p,c}} T_\mathrm{c} + \dot{m}_\mathrm{c} c_{\mathrm{p,}} dT_\mathrm{c} + d\dot{q}_\mathrm{loss,ss} \quad (9)$$

The radiation term in the particle and wall energy balance equation is based on a particle numbering up approach. The number of particles within each control volume segment is calculated from the solid volume fraction, which is a function of the particle mass flow rate, velocity, density, and cross-sectional area. All these parameters are constant, as the velocity of particles is assumed constant at 0.18 m s^{-1}.

To calculate the convection heat transfer between the particle/air mixture and the wall, a heat transfer coefficient based on the Nusselt number for fully developed laminar flow in a straight tube is used, shown in Equation (10).

$$Nu_\mathrm{a,w} = \frac{\alpha_\mathrm{a,w} d_\mathrm{in,inner}}{C_1 k_\mathrm{air}} = 4.36 \quad (10)$$

The variable C_1 in Equation (10) is an empirically derived enhancement factor to account for the increased thermal conductivity of the air stream, which is shown to increase in particle laden flows first reported by Maxwell [30] and further investigated by Kumar and Murthy in [31]. The effective heat transfer enhancement is reported to increase between 10% - 15% for randomly arranged particles with a solid volume fraction of 4.3%, nearly dilute conditions [31]. In the model, the

DOI: 10.17185/duepublico/83285

enhancement factor used is 3 because not only is the thermal conductivity of the air slightly increasing, but the convective heat transfer of a laminar flow also increases when flowing through a static mixing tube, as reported by Rahmani et al. in [32]. Rahmani et al. found that for flows with Re=100, the measured heat transfer coefficient of a laminar flow through a static mixer was on average increased by over 100%. Local increases up to 200% were reported at the interfaces of the static mixing elements. The experimental setup in [32] had 6 static mixing elements, the heat exchanger here has 32, therefore the assumption that heat transfer from the air to the wall is enhanced by a factor of 3 from both the increased thermal conductivity due to the particles in the flow and the enhancement from mixing in the tube can be treated as valid. The air thermal conductivity is evaluated in each control volume segment using the local temperature of the particles.

Other boundary and initial conditions were set to match the conditions used in the experiments. The measured steady state heat loss of the sCO_2 flow was incorporated into the energy balance equation for the sCO_2 flow, and a UA value of 0.2 W K^{-1} was added to the particle flow to represent heat loss to the environment through radiation, convection, and conduction into the frame of the test section. An additional loss term is incorporated into the particle domain, which is the heat loss to the parasitic air stream for the trials with counterflow. This loss is calculated assuming the air temperature exiting the ERR is equal to the particle temperature entering, and the flow rate of the air is set based on the experimental condition. For flows with no counterflow, no heat loss is recorded into the air stream.

Figures 8 and 9 show the predicted versus measured heat transfer rates into/out of the particles and sCO_2, respectively. The mean absolute percentage error (MAPE, Eq. 11) and mean percent error (MPE, Eq. 12) for the particle heat transfer rate is 8.2% and 6.3%, respectively. Nearly all the model predicted cases fall within the ±15% error, and all are within experimental uncertainty. The model shows a trend of overpredicting the heat transfer rate of cases without counterflow air, likely due to underestimating the heat loss from the particle domain.

$$MAPE = \frac{100\%}{n}\sum_{n=1}^{n}\frac{|Predicted - Measured|}{Measured} \quad (11)$$

$$MPE = \frac{100\%}{n}\sum_{n=1}^{n}\frac{Predicted - Measured}{Measured} \quad (12)$$

For sCO_2, the MAPE and MPE are 9.7% and 4.5% respectively. The model predicts the results for all cases within the bounds of experimental uncertainty. A slight overprediction on the 200 °C sCO_2 temperature trials with high temperatures particles is also likely due to insufficient heat loss incorporated into the model. For the sCO_2 domain, the steady state heat loss at 200 °C was 30.3 W, the same value used during experimental data reduction. The model assumes the steady state heat loss is

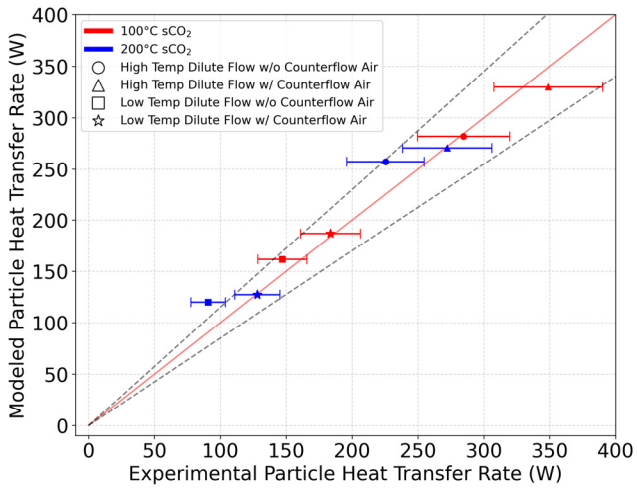

Figure 8: Comparison of predicated and measured particle heat transfer rates. Dashed lines represent ±15% error.

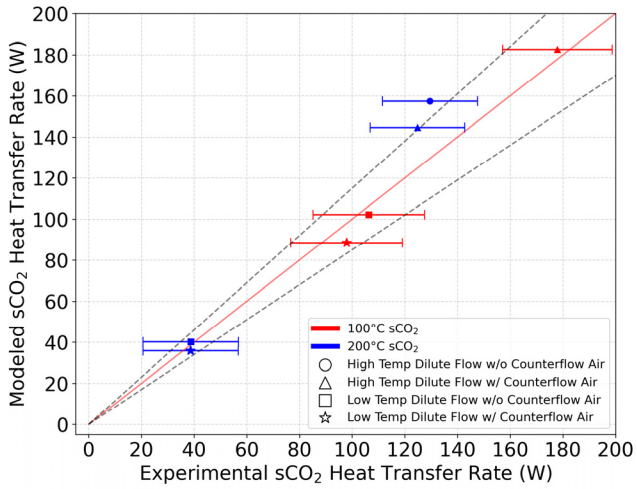

Figure 9: Comparison of predicated and measured sCO_2 heat transfer rates. Dashed lines represent ±15% error.

uniform throughout test section, when local heat loss is variable based on surface temperature and insulation thickness.

Overall, the predictive capability of the model shows agreement within experimental uncertainty for the parameters investigated. This 1-D model can be used for low-cost parametric sweeps of sCO_2 and particle inlet temperatures and flow rates to better understand operating conditions, especially at conditions near the design point for a particle-to-sCO_2 heat exchanger operating in a closed Brayton cycle.

CONCLUSIONS

This study successfully developed and demonstrated a supercritical carbon dioxide (sCO_2) test facility designed to simulate the inlet conditions of a primary heat exchanger in a recompression Brayton cycle. The facility was demonstrated to achieve temperatures up to 550°C at flow rates of more than 13 g s^{-1} and pressure of 9.33 MPa. Higher pressures can be achieved

DOI: 10.17185/duepublico/83285

by replacing the mass flow meter. The facility was used to evaluate the heat transfer performance of a novel particle-to-sCO_2 heat exchanger for concentrated solar power applications.

The experimental data validated thermal and hydraulic models, demonstrating their predictive capability within experimental uncertainty. These models can now be used to guide the design of larger-scale particle-to-sCO_2 heat exchangers, optimizing their performance for integration into next-generation concentrated solar power plants. Future work will focus on further enhancing the heat transfer rates by incorporating additional heat transfer area in the center tube and exploring the use of reactive particles.

NOMENCLATURE

α	Heat transfer coefficient (kW m^{-2} K^{-1})
A	Area (m^2)
c_p	Specific heat (kJ kg^{-1} K^{-1})
d	Diameter (m)
h	Specific enthalpy (kJ kg^{-1})
k	Thermal conductivity (W m^{-1} K^{-1})
L	Reactor height (m)
$\dot{m}$	Mass flow rate (kg s^{-1})
$\dot{Q}$	Heat transfer rate (kW)
T	Temperature (°C)
t	Time (s)
U	Overall conductance (kW K^{-1} m^{-2})

Subscripts

a	air
c	carbon dioxide
in	inlet
out	outlet
p	particle
rad	radiation
res	residence
rxn	reaction
w	wall

ACKNOWLEDGEMENTS

This material is based upon work supported by the U.S. Department of Energy's Office of Energy Efficiency and Renewable Energy (EERE) under the Solar Energy Technologies Office Award Number DE-EE0008991. The views expressed herein do not necessarily represent the views of the U.S. Department of Energy or the United States Government. **Full Legal Disclaimer**: This report was prepared as an account of work sponsored by an agency of the United States Government. Neither the United States Government nor any agency thereof, nor any of their employees, makes any warranty, express or implied, or assumes any legal liability or responsibility for the accuracy, completeness, or usefulness of any information, apparatus, product, or process disclosed, or represents that its use would not infringe privately owned rights. Reference herein to any specific commercial product, process, or service by trade name, trademark, manufacturer, or otherwise does not necessarily constitute or imply its endorsement, recommendation, or favoring by the United States Government or any agency thereof.

REFERENCES

[1] M. Mehos *et al.*, "Concentrating Solar Power Gen3 Demonstration Roadmap," 2017, [Online]. Available: http://www.nrel.gov/docs/fy17osti/67464.pdf

[2] K. J. Albrecht, H. F. Laubscher, M. D. Carlson, and C. K. Ho, "Development and Testing of a 20 kW Moving Packed-Bed Particle-To-sCO2 Heat Exchanger and Test Facility," pp. 1–6, 2021.

[3] T. Baumann and S. Zunft, "Development and Performance Assessment of a Moving Bed Heat Exchanger for Solar Central Receiver Power Plants," *Energy Procedia*, vol. 69, no. 0, pp. 748–757, 2015, doi: 10.1016/j.egypro.2015.03.085.

[4] P. Bartsch and S. Zunft, "Granular flow around the horizontal tubes of a particle heat exchanger: DEM-simulation and experimental validation," *Solar Energy*, vol. 182, pp. 48–56, Nov. 2019, doi: 10.1016/j.solener.2019.01.086.

[5] J. D. Hertel and S. Zunft, "Experimental validation of a continuum model for local heat transfer in shell-and-tube moving-bed heat exchangers," *Appl Therm Eng*, vol. 206, Nov. 2022, doi: 10.1016/j.applthermaleng.2022.118092.

[6] D. C. Miller, C. J. Pfutzner, and G. S. Jackson, "Heat transfer in counterflow fluidized bed of oxide particles for thermal energy storage," *Int J Heat Mass Transf*, vol. 126, pp. 730–745, 2018, doi: 10.1016/j.ijheatmasstransfer.2018.05.165.

[7] J. R. Fosheim *et al.*, "Narrow-channel Fluidized Beds for Particle- sCO2 Heat Exchangers in Next Generation CPS Plants," in *SolarPACES AIP Conference Proceedings 2445, 160007*, 2020.

[8] W. J. Arthur-Arhin, K. J. Brewster, A. Thompson, G. S. Jackson, K. J. Albrecht, and D. Amogne, "Demonstrating a 40-kWth , Counterflow Particle-sCO2 Narrow-Channel, Fluidized Bed Heat Exchanger," in *SolarPACES 2022*, 2022.

[9] J. R. Fosheim *et al.*, "Design of a 40-kWth counterflow particle-supercritical carbon dioxide narrow-channel fluidized bed heat exchanger," in *SolarPACES*, 2023. doi: 10.1063/5.0165673.

[10] Z. Ma and J. Martinek, "Fluidized-bed heat transfer modeling for the development of particle/supercritical-CO2 heat exchanger," in *ASME 2017 11th International Conference on Energy Sustainability, ES 2017*, 2017, pp. 1–10. doi: 10.1115/ES2017-3098.

[11] Z. Ma and J. Martinek, "Analysis of a fluidized-bed particle/supercritical-CO2 heat exchanger in a concentrating solar power system," *Journal of Solar Energy Engineering, Transactions of the ASME*, vol. 143, no. 3, 2021, doi: 10.1115/1.4048548.

[12] P. Steiner, K. Schwaiger, H. Walter, M. Haider, and M. Hammerle, "Fluidized Bed Particle Heat Exchanger for

DOI: 10.17185/duepublico/83285

Supercritical Carbon Dioxide Power Cycles," in *Proceedings of the ASME 2016 International Mechanical Engineering Congress and Exposition*, 2016. [Online]. Available: http://asmedigitalcollection.asme.org/IMECE/proceedings-pdf/IMECE2016/50688/V014T07A014/4270287/v014t07a014-imece2016-67104.pdf

[13] S. Thanheiser, M. Haider, and P. Schwarzmayr, "Experimental Investigation of the Heat Transfer between Finned Tubes and a Bubbling Fluidized Bed with Horizontal Sand Mass Flow," *Energies (Basel)*, vol. 15, no. 4, Nov. 2022, doi: 10.3390/en15041316.

[14] B. J. Siefering, M. Umer, E. B. Stechel, and B. M. Fronk, "Thermodynamic Analysis of a Reactive Particle-to-sCO2 Heat Exchanger for Recovering Stored Thermochemical Energy," in *5th European supercritical CO2 Conference*, 2023.

[15] M. Umer, B. J. Siefering, and B. M. Fronk, "Numerical Investigation of Hydrodynamic and Thermal Performance of Gravity Driven Dilute Flow in a Straight Channel," in *8th Thermal Fluids Engineering Conference*, 2023.

[16] B. Siefering, "Investigation of a Dilute Flow Particle Reactor for Coupling Thermochemical Energy Storage to Supercritical Carbon Dioxide Brayton Cycles," Ph.D., The Pennsylvania State University, University Park, PA, 2024. Accessed: Nov. 13, 2024. [Online]. Available: https://etda.libraries.psu.edu/catalog/28254bjs6878

[17] ASME, *Process Piping ASME Code for Pressure Piping, B31.3*. 2022.

[18] R. Span and W. Wagner, "A new equation of state for carbon dioxide covering the fluid region from the triple-point temperature to 1100 K at pressures up to 800 MPa," *J Phys Chem Ref Data*, vol. 25, no. 6, pp. 1509–1596, 1996, doi: 10.1063/1.555991.

[19] C. C. Inc., "CARBOHSP Technical Data Sheet," 2022.

[20] N. P. Siegel, M. D. Gross, and R. Coury, "The development of direct absorption and storage media for falling particle solar central receivers," *J Sol Energy Eng*, vol. 137, no. 4, pp. 1–7, 2015, doi: 10.1115/1.4030069.

[21] STEEL Lab, "Thermophysical Properties Database of Gen3 CSP Materials," https://gen3csp.gatech.edu/.

[22] Carbo Ceramics Inc., "CARBOHSP Technical Data Sheet," 2022.

[23] S. J. Kline and F. A. McClintock, "Describing uncertainties in single-sample experiments," *Mech. Eng.*, vol. 75, pp. 3–8, 1963.

[24] G. Nellis and S. Klein, *Heat Transfer*. New York: Cambridge University Press, 2009.

[25] M. Umer, B. J. Siefering, and B. M. Fronk, "Experimental investigation of Multi-Mode heat transfer to a Free-Falling dilute particle cloud in a heated vertical tube," *Exp Therm Fluid Sci*, vol. 159, p. 111278, Dec. 2024, doi: 10.1016/j.expthermflusci.2024.111278.

[26] K. J. Albrecht, M. D. Carlson, H. F. Laubscher, R. Crandell, N. DeLovato, and C. K. Ho, "Testing and model validation of a prototype moving packed-bed particle-to-sCO2 heat exchanger," in *AIP Conference Proceedings 2303, 030002 (2020)*, AIP Publishing, 2020. doi: 10.1063/5.0031483.

[27] K. J. Albrecht, H. F. Laubscher, M. D. Carlson, and C. K. Ho, "Development and testing of a 20 kW moving packed-bed particle-to-sCO2 heat exchanger and test facility," in *Proceedings of the ASME 2021 15th International Conference on Energy Sustainability, ES 2021*, 2021. doi: 10.1115/ES2021-64050.

[28] M. J. Frain, D. P. Schmidt, and W. A. Fiveland, "An experimental investigation of the influence of gas and solid particle interaction on the heat transfer effectiveness of a falling-bed heat exchanger," *J Heat Transfer*, vol. 127, no. 10, pp. 1077–1086, Oct. 2005, doi: 10.1115/1.2033904.

[29] K. S. Rajan, S. N. Srivastava, B. Pitchumani, and B. Mohanty, "Simulation of countercurrent gas-solid heat exchanger: Effect of solid loading ratio and particle size," *Appl Therm Eng*, vol. 27, no. 8–9, pp. 1345–1351, Jun. 2007, doi: 10.1016/j.applthermaleng.2006.10.026.

[30] J. C. Maxwell, *A treatise on electricity and magnetism*, vol. 1. Oxford: Clarendon Press, 1873.

[31] S. Kumar and J. Y. Murthy, "A numerical technique for computing effective thermal conductivity of fluid-particle mixtures," *Numerical Heat Transfer, Part B: Fundamentals*, vol. 47, no. 6, pp. 555–572, Jun. 2005, doi: 10.1080/10407790590928937.

[32] R. K. Rahmani, T. G. Keith, and A. Ayasoufi, "Numerical study of the heat transfer rate in a helical static mixer," in *Journal of Heat Transfer*, 2006, pp. 769–783. doi: 10.1115/1.2217749.

DOI: 10.17185/duepublico/83285

DOI: 10.17185/duepublico/83285
URN: urn:nbn:de:hbz:465-20250428-091728-3